RESEARCH ARTICLE

Semi-idealized simulations of wintertime flows and pollutant transport in an Alpine valley. Part II: Passive tracer tracking

Tiphaine Sabatier[ID] | Yann Largeron | Alexandre Paci | Christine Lac | Quentin Rodier | Guylaine Canut | Valéry Masson

Centre National de Recherches Météorologiques, Université de Toulouse, Météo-France, CNRS, Toulouse, France

Correspondence
T. Sabatier, CNRM, Université de Toulouse, Météo-France and CNRS, 42 av. Gaspard Coriolis, 31057, Toulouse, France.
Email: tiphaine.sabatier@gmail.com

Funding information
The French Ministry of higher education and research, CNRS (Centre National de la Recherche Scientifique) and Météo-France

Abstract

Under wintertime quiescent conditions, thermally driven circulations represent one of the only sources of tracer dispersion over mountainous terrain. Those circulations can be unequally developed at a valley scale since they strongly depend on local morphological arrangement. At the same time, very heterogeneous pollutant distribution can be observed, as for instance in a French Alpine basin located in the Arve River valley. This complex basin regularly shows large variations in pollutant concentrations with certain sectors suffering from poor wintertime air quality. On the other hand, the surrounding tributary valleys appear to be less affected, suggesting that the basin local dynamics may participate in pollutant trapping. The present study intends to classify the pollutant transport mechanisms in terms of efficiency and to identify the most dynamically vulnerable atmospheric volumes regarding pollutant accumulation. This is achieved through a set of semi-idealized high-resolution numerical simulations reproducing a full diurnal cycle with passive tracers released continuously at a constant rate. The model is used as a laboratory in order to quantify the influence of several processes on transport mechanism efficiency. This approach underlines the high efficiency of vertical transport by anabatic winds while horizontal transport efficiency by up-valley wind systems remains weak, leaving the surrounding tributary valleys almost unaffected by the basin pollution during daytime. At night, the efficiency of horizontal transport by the down-valley wind systems depends on the tracer source location within the basin. In addition, the tracers emitted within the tributary valleys do not reach the basin bottom because of thermal stratification and local morphological arrangement but rather degrade the air quality of mid-altitude villages lying along the basin sidewalls.

KEYWORDS
atmospheric boundary layer, complex terrain, local dynamics, passive tracer, semi-idealized numerical simulation, wintertime air quality

1 | INTRODUCTION

Urbanized Alpine valleys frequently suffer from poor air quality under wintertime anticyclonic conditions (Malek *et al.*, 2006; Silcox *et al.*, 2012; Largeron and Staquet, 2016; VanReken *et al.*, 2017). Those situations are characterized by strong temperature inversions, also referred to as cold air pools, which considerably reduce the vertical mixing (Whiteman *et al.*, 2001; Lareau *et al.*, 2013) thereby favouring the pollutant accumulation in the near-surface atmosphere (Pernigotti *et al.*, 2007; Harnisch *et al.*, 2009; Perrino *et al.*, 2014; Whiteman *et al.*, 2014; Lehner and Rotach, 2018). Under these conditions, local thermally driven circulations are one of the main drivers of pollutant redistribution and allow some degree of ventilation (Schäfer *et al.*, 2008; Gohm *et al.*, 2009; Pardyjak *et al.*, 2009; Diémoz *et al.*, 2019). Under clear-sky conditions, those circulations are characterized by a wind reversal twice per day at the slope and valley scales (Defant, 1949; Zardi and Whiteman, 2013). During the daytime period, local flows are orientated up-slope and then reverse to down-slope at night (Whiteman, 2000). The influence of the daytime dynamics on pollutant transport has been thoroughly investigated through idealized numerical studies. At the slope scale, anabatic winds represent a mechanism of vertical transport (Henne *et al.*, 2004; Leukauf *et al.*, 2015), which can be more effective than convection (Rotach *et al.*, 2014) but which may also recirculate the pollutants toward their sources when associated with a return branch (Rendón *et al.*, 2015). The vertical transport efficiency depends on the atmosphere state and radiative forcing (Leukauf *et al.*, 2016) and on the land cover which drives the surface albedo (Lehner and Gohm, 2010). In particular, several studies have underlined the role of a snow cover which favours the near-surface pollutant accumulation (Chazette *et al.*, 2005; Whiteman *et al.*, 2014). At the valley scale, Wagner *et al.* (2015a; 2015b) highlighted the along-valley flow dependence on topographic characteristics such as valley width and bottom inclination while Lang *et al.* (2015) discussed the impact of valley floor heights on tracer export. The valley orientation also appears as a key parameter since it governs the short-wave incoming radiation and may generate an asymmetry in the pollution distribution between sunlit and shadow sidewalls, as reported by Bader and Whiteman (1989), Chazette *et al.* (2005) and Gohm *et al.* (2006). The thermally driven flows developed at night may recirculate the pollutants toward their emission sources (Steyn *et al.*, 2013), but they may also represent a source of mixing that favours the plume dispersion (Gudiksen and Shearer, 1989; O'Steen, 2000). As a result, the pollutant dispersion in mountainous terrain is complex because of topographic effects which generate multi-scale transport processes (Adler and Kalthoff, 2014; Lehner and Rotach, 2018; Serafin *et al.*, 2018). These local dynamics may induce a more degraded air quality than would be expected over flat terrain considering the same emissions (Steyn *et al.*, 2013).

For the present study, we address the question of the impact of local flows on pollutant transport over a complete diurnal cycle in the Arve River valley situated close to Mont Blanc in the French Alps. A part of this valley was investigated during the Passy-2015 field experiment which aimed to understand the role of the dynamics on wintertime pollution episodes which frequently affect the area (Paci *et al.*, 2016). This part of the Arve River valley can be decomposed into several sectors, as can be seen in Figure 1a with a central billhook basin shape connected with three tributary valleys (Megève, Saint-Gervais and Chamonix) and a downstream wider part. The air quality monitoring performed by the local Atmo-Auvergne Rhone Alpes agency shows that local heterogeneities in the pollutant concentrations are reached within those sectors (Atmo-AURA, 2016). In particular, high PM10 concentrations are frequently measured at the Passy and Sallanches stations, both located at the basin bottom. These dynamics are illustrated in Figure 2a representing the time cycle of PM10 concentrations measured during the first Intensive Observation Period (IOP1) of the field experiment. This IOP1 combined all the favourable conditions for pollution accumulation with wintertime radiative forcing, clear-sky conditions and persistent temperature inversion (Sabatier *et al.*, 2018). The basin stations are both associated with a two-peak diurnal cycle with the highest concentrations measured at Passy. In comparison, the PM10 concentrations measured at Chamonix appear lower than those recorded within the basin. As spring approaches, the inter-station variation is reduced, as can be seen in Figure 2b representing the time cycle of PM10 concentrations from 7 to 13 March 2015. This evolution raises the question of the relative impact of physical mechanisms at work between those two months since the PM10 concentrations result from the combination of the atmospheric conditions (thermal structure and wind circulation), the dynamics of emissions and the life cycle of particles whose relative contributions must be assessed separately (Kalthoff *et al.*, 2000; Kukkonen *et al.*, 2005; Steyn *et al.*, 2013). In this work, our attention is focused on the atmospheric conditions by considering passive tracers which are not subjected to sedimentation processes or chemical reactions. One of our goals is to give quantitative insights in order to estimate to what extent atmospheric conditions could be responsible for both the pollutant accumulation within the basin and the basin-scale heterogeneity in pollutant concentrations.

The characterization of the local circulations developed during the IOP1 has been proposed from scanning
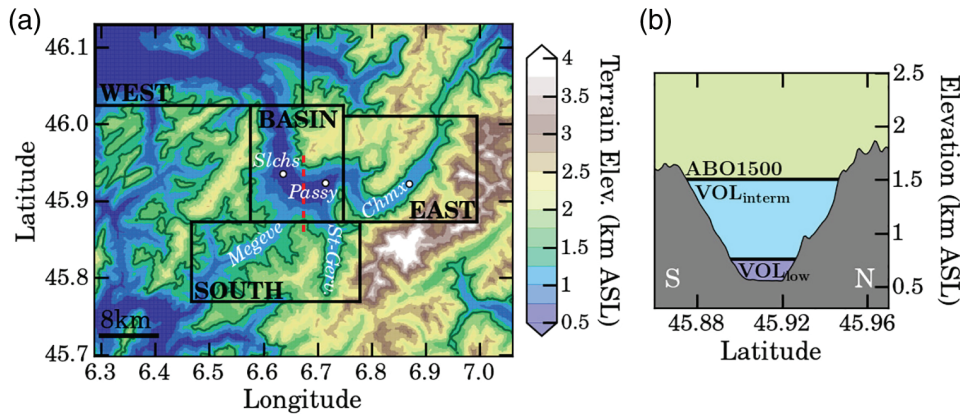
FIGURE 1 (a) Domain of simulation with the four sub-domains (black boxes) used to compute the tracer tracking. Main places are indicated in white and emission sources of passive tracers by white dots. The grey line denotes the 1,500 m asl elevation. (b) Vertical separation of the basin atmosphere along the south–north cross-section drawn in red in (a)
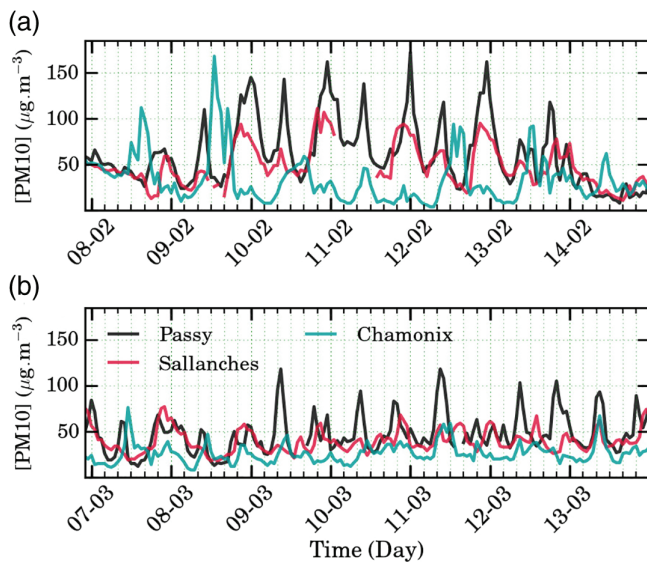

FIGURE 2 Hourly PM10 concentrations measured at three stations located in the Arve River valley (Figure 1a shows the station locations) during (a) the IOP1 of the Passy-2015 field experiment in February 2015 and (b) a second anticyclonic episode documented during the field experiment in March 2015

The determination of the influence of the local wind dynamics on pollutant transport is the objective of the present study. This information is valuable for the implementation of effective regulations under degraded air quality conditions (Whiteman *et al.*, 2014). For this purpose, passive tracer analyses are conducted in order to combine the information of tracer spatial distribution with the circulation features described in Part I. The same set of numerical experiments are used to perform tracer tracking by dividing the atmosphere into near-surface, intermediate and upper sub-volumes for each valley composing the area. Passive tracers are emitted continuously at a constant rate in three places associated with different wind dynamics as shown in Part I. The choice of the point sources does not intend to be representative of the main emission spots but rather to investigate how the local dynamics drive the tracer distribution over the area. More precisely, this framework allows us to address the following questions :

- Among the characteristics of the dynamics described in Part I, which ones play a major role on tracer transport? What is the relative influence of the along-slope and along-valley circulations?

- How are the tracers distributed between the atmospheric volumes composing the valleys dependent on the emission source location? More precisely, to what extent are the tracers emitted (a) in the Chamonix valley incorporated within the basin, and (b) within the basin evacuated toward the tributary valleys?

- What role do the early-spring (March) solar forcing, the initial stability and the snow cover play in the trapping of pollutants within the near-surface atmosphere?

The paper is organized as follows: the main results from Part I are summarized in Section 2. The set of numerical experiments along with the tracer tracking methodology are presented in Section 3. The tracer tracking is proposed in Section 4 for the reference simulation,

Doppler Lidar observations by Sabatier *et al.* (2018). Then, a numerical study was performed in a companion paper (Sabatier *et al.*, 2019) whicht will be referred to as Part I hereafter. In Part I, a high-resolution numerical simulation was run in a semi-idealized framework (i.e. no large-scale coupling and initial atmosphere at rest) with the non-hydrostatic anelastic atmospheric research model Meso-NH (Lac *et al.*, 2018). This simulation was intended to reproduce simplified conditions encountered during the IOP1 in order to improve our understanding of the observed wind structures. In addition, various numerical experiments were conducted in order to quantify to what extent the circulations are modified by weaker initial stratification, higher radiative forcing or snow cover and to better understand the mechanisms driving local circulations in this complex valley.
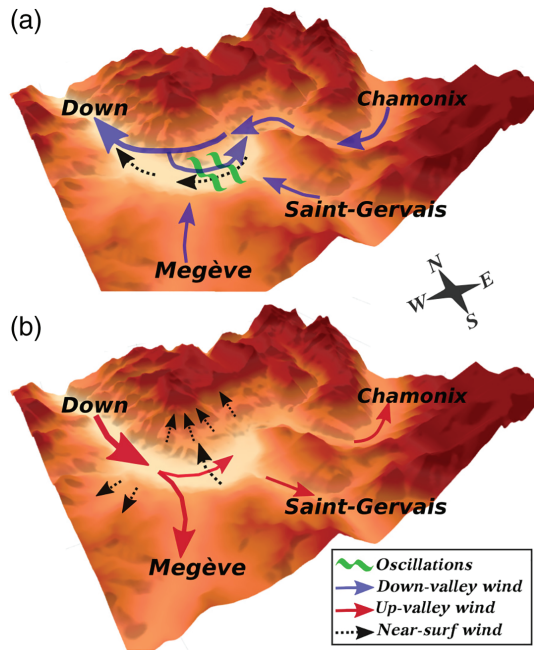
FIGURE 3 Conceptual schemes of the main wind structures highlighted in Part I during the (a) night-time and (b) daytime periods

while process analysis is described in Section 5. A general discussion is offered in Section 6, while the main conclusions are drawn in Section 7.

2 | MAIN FEATURES OF THE WIND DYNAMICS

The main findings of Part I are illustrated in Figure 3 for (a) night-time and (b) daytime circulations. At night, a three-layer wind structure is developed within the basin with (a) a near-surface down-valley wind developed over a few tens of metres (in black in Figure 3a,b) an intermediate quiescent layer submitted to wind direction oscillations (in green), and (b) an upper down-valley wind with a jet-like structure and a jet nose around 250 m above ground level (in blue). The near-surface down-valley wind has a local origin while the upper one results from the convergence of drainage flows from the tributary valleys. These flows cannot plunge toward the near-surface basin atmosphere due to the combination of inertia and strong near-surface inversion. This three-layer structure evolves between the curved central part of the basin and the linear western branch. In the central part, the quiescent intermediate layer prevails over the near-surface down-valley flow, whose average intensity remains lower than $0.5\,\mathrm{m\cdot s^{-1}}$, while in the western linear branch the quiescent layer almost disappears because of a more developed near-surface system. As a consequence, a gradual

increase of the recirculation is observed from the west to the east of the basin (following the indices definition of Allwine and Whiteman, 1994). The process analysis revealed that the near-surface down-valley wind depends on the atmospheric stability and becomes more intense as the stability decreases.

During the daytime period, the anabatic winds mainly develop along the south- and east-facing basin sidewalls under the February radiative forcing (in black in Figure 3b). This along-slope circulation drives the near-surface circulation with a southerly wind layer developed in the first tens of metres at the basin centre over the 1000–1700 UTC period. The anabatic winds appear sensitive to the presence of snow cover (which reduces their intensity) and to the radiative forcing (where a lengthening of the anabatic regime under March solar conditions leads to a wider area impacted). At the valley scale, a mass budget computation has shown that in February the airmass entering the basin from the downstream section represents approximately half of the total basin airmass. Among this incoming airmass, more than half is vented out by the Megève tributary valley, leading to weak mass fluxes toward the eastern part of the basin and the Saint-Gervais and Chamonix valleys (in red). In March, the higher radiative forcing leads to an intensification of the up-valley wind systems flowing through the basin and the tributary valleys, along with a more equilibrated distribution of the airmass flowing through the three tributary valleys.

3 | METHODOLOGY

3.1 | Numerical configuration

A set of high-resolution numerical simulations are performed with the non-hydrostatic anelastic atmospheric research model Meso-NH (Lac *et al.*, 2018). Simulations are run over the domain presented in Figure 1a, which covers an area of $60\times48\,\mathrm{km^2}$ with a horizontal grid spacing of 100 m. In the vertical, the grid is decomposed into 72 levels using a terrain-following coordinate system (Gal-Chen and Somerville, 1975), with a 2 m resolution at the first level, a stretching of 10% in the first 1,000 m and 20% aloft. The simulations are initialized in a semi-idealized framework by considering a realistic orography provided from the 90 m resolution Shuttle Radar Topography Mission (SRTM) database and a simplified atmospheric initial state. More precisely, potential temperature and humidity profiles are specified at the basin centre and then interpolated horizontally and vertically over the entire grid. For the wind, the initial state is a zero-wind profile and there is no large-scale tendency.

Turbulence scheme	3D scheme; Cuxart *et al.* (2000)
	Mixing length; Deardorff (1974)
Radiation scheme	Short-wave; Fouquart and Bonnel (1980)
	Long-wave; Mlawer *et al.* (1997)
Surface scheme	SURFEX; Masson *et al.* (2013)
Surface initialization	Orography: SRTM database (90 m resolution)
	Land use: ECOCLIMAPII; Faroux *et al.* (2013)
Boundary conditions	Open; Carpenter treatment (equation 6 of Lac *et al.*, 2018)

TABLE 1 Summary of the numerical set-up. More details can be found in Part I.

This approach allows us to focus on local dynamics. The simulations are initialized at 0900 UTC and integrated for a 39 hr period, covering the full diurnal cycle of the second day. A model time step of 1 s is applied. The tracers, as well as meteorological scalar variables, are advected with the PPM scheme (Colella and Woodward, 1984), while the momentum field is transported with a fourth-order centred scheme and a fourth-order Runge–Kutta temporal scheme, allowing a fine effective resolution (around $5\Delta x$ according to Ricard *et al.*, 2013). A brief description of the model parametrization is given in Table 1.

3.2 | Numerical experiments

The simulation of reference (REF) is considered as representative of wintertime local pollution event based on conditions encountered during the IOP1 of the Passy-2015 field experiment (10–12 February 2015). The atmosphere is initialized from potential temperature and humidity profiles measured at 0900 UTC on 11 February by radiosondes (profiles in figure 2 of Part I). In Part I, the REF simulation was used as a reference for comparison with numerical experiments designed in order to determine the influence of several processes (snow cover, radiative forcing, initial stability profile) on wind dynamics. In addition, the comparison with observations underlined the model ability in reproducing the main features of the dynamics in spite of the numerical simplifications. This confirms that the observed dynamics are mainly local, as expected under persistent temperature inversion conditions (Whiteman, 2000). The same set of simulations is used in the present study in order to quantify the relative influence of processes on pollutant dispersion and therefore to identify the most relevant dynamics features for air quality. Table 2 gathers the differences in numerical configurations between the set of experiments and the REF simulation. The simulation spin-up is short (around 2 hr) and a steady state is rapidly reached and maintained during the rest of the simulation.

TABLE 2 Numerical experiments and differences from the REF simulation

	Differences with respect to the REF simulation
LESSstable	Lower stability with an initial Brunt–Väisälä frequency in the first 500 m above ground level of $0.023\,s^{-1}$ instead of $0.032\,s^{-1}$ in REF (atmosphere initialisation from a temperature profile measured at 0900 UTC on 9 March instead of 0900 UTC on 11 February for REF).
MARCH	Stronger solar forcing (9 March instead of 11 February for REF).
SNOW	Addition of a 30 cm thick snow cover over the entire domain.
SNOWsouth	Addition of a 30 cm thick snow cover restricted to the southern north-facing shaded slopes of the basin.

3.3 | Tracer tracking

The present study is based on a tracer tracking analysis performed over the simulation domain displayed in Figure 1a. This domain is decomposed into four sub-domains associated with the main valleys of interest. The central BASIN domain includes the curved and linear parts of the basin. The WEST domain corresponds to the wider downstream part of the valley. The EAST domain is associated with the Chamonix valley and the SOUTH domain gathers the two tributary valleys lying in the southern sidewall of the basin (Megève and Saint-Gervais). These four domains are vertically marked out at 1,500 m above sea level (asl), this altitude being the average elevation of the capping inversion during the stagnation stage of IOP1 (not shown). The domains are then split into two sub-volumes displayed in Figure 1b; the first one near the surface (VOL_{low}) and the second one (VOL_{interm}) representing the intermediate volume between VOL_{low} and 1,500 m asl. A fixed elevation threshold is used to vertically mark out these two sub-volumes, this method being the more appropriate due to the high degree of orographic complexity. In

order to account for the variations in bottom valley elevations, these thresholds are adapted and set to 760 m asl in the WEST and BASIN domains and 1,250 m asl in the SOUTH and EAST domains, representing an average thickness of approximatively 200 m above the respective average valley bottom elevations. In addition to these eight volumes, an upper volume is defined by considering all the grid cells above 1,500 m asl (ABO1500). This three-layer decomposition allows us to clearly differentiate the near-surface atmosphere usually associated with the highest population density, the upper atmosphere for which the influence of local orography is reduced, and an intermediate atmospheric layer.

Starting from this domain decomposition, the tracer tracking is performed so as to identify the volumes affected by pollution depending on the source location. Passive tracers are emitted at the ground level from three source points (Passy, Sallanches, Chamonix) indicated by white dots in Figure 1a. For each source, the tracers are released continuously over the 39 hr of simulation at an arbitrary constant rate $Q_{emis} = 25.64$ kg·hr^{-1} leading to a total mass of 1,000 kg per source at the end of the simulation. Lateral boundaries being opened, tracers can escape, meaning their mass is not conserved. In the present case, the remaining masses at the end of the reference simulation are equal to 886, 883 and 830 kg for tracers emitted at Passy, Sallanches and Chamonix respectively.

Normalized tracer masses (M_T expressed in %) are derived by summing the mass of tracer present in all the grid cells composing each sub-volume according to

$$M_T(t) = 100 \frac{\sum_{vol} \rho_{air} V_{air} R_T}{Q_{emis} \, t},$$
(1)

with t the time duration from the beginning of the simulation, V_{air} and ρ_{air} the volume and density of dry air and R_T the tracer mixing ratio. In addition, normalized tracer masses are derived within the entire domain of simulation (ALL).

Because of the passive nature of tracers (chemical reactions and sedimentation are not considered), tracer mass fluctuations within a volume are due only to mixing or advection by local flows. Among the different ways on which the latter can develop, the present study focuses on the three mechanisms:

- the *vertical transport* by anabatic winds which drives the tracers along the slopes and may extract them from the valley atmosphere;
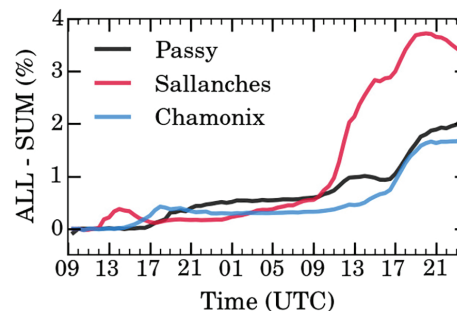

FIGURE 4 Temporal evolution of the difference of tracer mass computed in the ALL and SUM volumes for the three emission sources in the reference simulation

- the *upstream transport* by the up-valley wind systems developed during the daytime period which may transfer the tracers from the basin toward the Chamonix, Saint-Gervais and Megève tributary valleys;

- the *downstream transport* induced by the down-valley wind developed at night which may advect the tracers toward the (more open) downstream part of the valley.

Hereafter, we present a quantification of the relative importance of these three types of transport in the region of interest during local pollution events based on the conditions encountered during the Passy-2015 field experiment. The analysis of the tracer mass distribution, along with the wind dynamics study proposed in Part I, will allow us to determine the actual impact of wind dynamics on tracer transport within a given valley from one layer to another and between the different valleys.

Note that, since the four considered domains (WEST, EAST, SOUTH, BASIN) do not cover the entire domain of simulation (cf. Figure 1a), the sum of the tracer mass within each of these subdomains (SUM) is not strictly equal to the total mass of tracer present within the entire domain of simulation (ALL). Figure 4 illustrates the time evolution of the difference between ALL and SUM over the 39 hr of simulation in the reference simulation. For every source, the difference progressively increases until the end of the simulation, reaching 2% for tracers emitted at Passy and Chamonix. The maximum difference concerns the tracers emitted at Sallanches which is mainly due to the proximity between the western side of the BASIN domain and the western sidewalls of the basin. However, this maximum never exceeds 4% of the total tracer mass emitted within the domain, allowing the decomposition to be validated to answer the questions introduced at the beginning of the study.
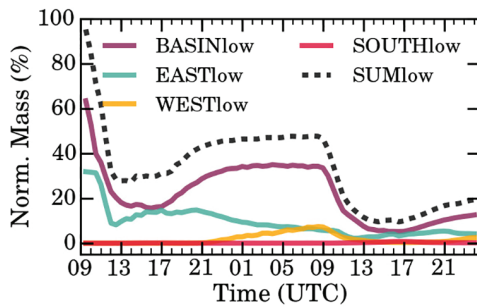
FIGURE 5 Temporal evolution of the total normalized mass of tracer (three emission sources combined) in the lowest near-surface volumes defined in Section 3.3 for the reference simulation. The dashed black curve represents the sum of the four sub-volumes

4 | TRACER TRANSPORT IN THE REFERENCE SIMULATION

4.1 | Mass accumulation in the lower volumes

The starting point of this analysis is proposed from Figure 5 which aims to compare the tracer accumulation within each valley composing the area for the reference simulation. This figure represents the time evolution of the total tracer mass (three sources combined) in the four lower volumes ($BASIN_{low}$, $EAST_{low}$, $WEST_{low}$, $SOUTH_{low}$). This focus on lower volumes gives insights into the relative level of exposure of the population living in the 200 m above the valley bottom in the four distinct domains considered. For this figure and all the following, the time series are plotted over the entire simulation duration (39 hr) in order to visualize how the tracers are transferred from one domain to another. However, the first hours of the series will not be analysed in details since it takes a few hours for the dynamics to establish.

The dashed black curve represents the sum of all the tracers present in the four lower volumes. At the beginning of the simulation, 100% of the mass is in the lower volumes since tracers are emitted at the ground level (66% within $BASIN_{low}$ which gathers two emission sources over three and 33% within $EAST_{low}$ which includes the third emission source). In the early morning of the second day (0900 UTC), 47% of the total mass is in the lower volumes while only 10% remains in the afternoon. This evolution is a clear indicator of the existence of effective transport mechanisms.

The decomposition per sub-domain shows that the tracer mass evolution differs from one valley to another. In the $BASIN_{low}$ volume, the tracer mass is systematically higher than in the upstream and downstream valley parts ($EAST_{low}$ and $WEST_{low}$ volumes respectively). In

particular, a factor of 5 is observed in the early morning of the second day (0900 UTC) between the $BASIN_{low}$ and $EAST_{low}$ volumes, while there is only a factor of 2 in emission sources (Passy and Sallanches in $BASIN_{low}$ versus Chamonix in $EAST_{low}$). This difference indicates a tracer accumulation rate that is 2.5 stronger within the BASIN than in the EAST domain for constant and equal emission rates.

In the $SOUTH_{low}$ volume, the tracer mass never exceeds 1%, meaning that this part of the domain is almost unaffected by the pollutants emitted at the three point sources. The same observation is valid for the $SOUTH_{interm}$ volume in which the maximum tracer mass is equal to 1.2% (not shown). These weak values mean that the up-valley winds developed during the daytime period in the Megève and Saint-Gervais valleys (Figure 3b) do not represent an effective mechanism of pollutant transport, thereby indicating that other mechanisms prevail (see next section).

4.2 | Decomposition per source

In the current section, the mass distribution between the lower and intermediate volumes are analysed for each tracer source independently. Figure 6 represents the time evolution of the normalized mass present in every sub-volume for tracers emitted at Passy, Sallanches and Chamonix (a, b, c respectively). In order to avoid overloaded figures, the $SOUTH_{low}$ and $SOUTH_{interm}$ volumes are not represented since the associated tracer masses are always lower than 2%, as shown in the previous section. The sums of the mass present within the seven sub-volumes are represented by dashed black curves and give an insight on the time evolution of the mass exported out of the closely examined volumes as mentioned in Section 3.3. The analysis is separated into two steps: (1) the comparison of the mass distribution for tracers emitted within the basin at Passy and Sallanches, and (2) the difference in behaviour for tracers emitted in the Chamonix valley.

4.2.1 | Tracers emitted within the basin

During the night-time period (2100–0800 UTC), the maximum of mass in the $BASIN_{low}$ volume is reached in the evening for Sallanches tracers (50% of mass at 2230 UTC of day 1) while it occurs in the early morning for Passy tracers (54% of mass at 0900 UTC of day 2). In addition, the night-time trends differ for the two sources with (a) a diminution of the Sallanches tracer mass over the entire night (mean slope = $-0.92\%\,hr^{-1}$ between 2100 and 0900 UTC) indicating that ventilation toward outer
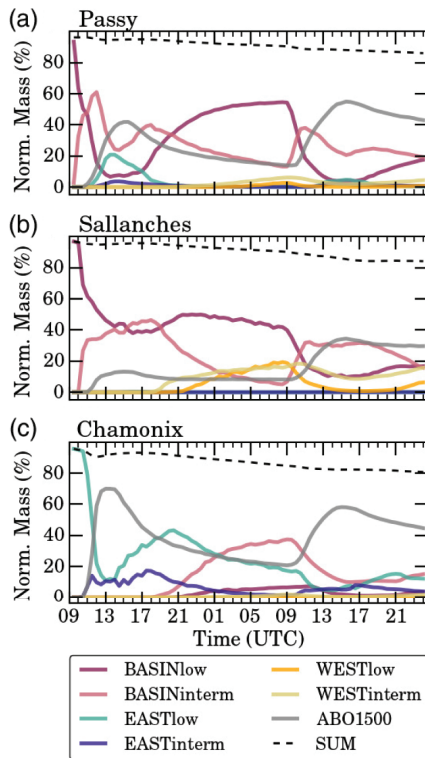
FIGURE 6 Temporal evolution of the normalized tracer mass within sub-volumes defined in the Section 3.3 determined for tracers emitted at (a) Passy, (b) Sallanches and (c) Chamonix in the reference simulation. The dashed SUM curve represents the addition of the seven coloured curves

domains prevails over mass accumulation within the basin, and (b) an increase of the Passy tracer mass (mean slope = $1.42\%\,hr^{-1}$ between 2100 and 0900 UTC) indicating a night-time accumulation within the $BASIN_{low}$ volume. This difference results from the downstream transport (BASIN→WEST) which mainly concerns the Sallanches tracers with 37% of mass in the $WEST_{low+interm}$ domain at 0900 UTC. This mechanism slightly affects the Passy tracers with only 9% of the mass in $WEST_{low+interm}$ at 0900 UTC. The mass export toward the WEST domain is about four times stronger for tracers emitted at Sallanches than at Passy.

This evolution is partly explained by the shorter distance between Sallanches and the western basin exit ($D_{slchs-exit} \simeq 16\,km$) while Passy is 8 km further east following the basin curvature, representing a ratio $\frac{D_{passy-exit}}{D_{slchs-exit}} = 1.5$. This is the maximum ratio of mass exported that could be reached if the down-valley wind was homogeneously developed along the basin axis. The ratio of 4 therefore indicates an evolution in the dynamics between the two parts of the basin which favours the export of Sallanches tracer. This is in agreement with some conclusions of Part I where we have shown that during the night (a) the

near-surface down-valley flow is more established in the western linear branch, while wind direction oscillations prevail in the central curved part of the basin and (b) the elevated down-valley wind is more established over the valley width in the western branch of the basin, while a recirculation cell develops in the curved sector. In addition, the recirculation index derived within the first 100 m above the ground has emphasized a gradual increase of stagnation from the west to the east of the basin (cf. figure 14 of Part I).

The central curved part of the basin is associated with wind oscillations (cf. figure 13 of Part I) which induce a back-and-forth motion of the tracer plume illustrated in Figure 7. This figure represents instantaneous fields of tracer mass (expressed in grams) every 30 min between 0230 and 0400 UTC for Passy and Sallanches tracers (cf. Figure 7a,b respectively). These fields allow us to visualize the spatial behaviour of the plumes which are determined as the total tracer mass present in the first 200 m above the ground. In addition, the 100 g contors are superimposed in black in order to facilitate the comparison between the two emission sources. For Passy tracers, a stagnation of the plume is observed with a back-and-forth motion of its western and eastern edges which limits the plume propagation in the down-valley direction (Figure 7a). On the other hand, the Sallanches plume front quickly evolves toward the downstream part of the valley and the tracer amount moving in the up-valley direction remains weak (Figure 7b).

From 0900 UTC of the second day of simulation, a mass transfer occurs from the lower to the intermediate basin volumes and then toward the ABO1500 volume highlighting an efficient vertical export (Figure 6a). This mechanism leads to an exponential decrease of the mass in $BASIN_{low}$ with a diminution from 54% at 0900 UTC to 3.9% at 1630 UTC for tracers emitted at Passy (Figure 6a). Note that a large part of this drop occurs in the time range 0900–1230 UTC. This decrease is due to the combination of convection and along-slope advection by anabatic winds. Figure 8 shows south–north cross-sections of mixing ratio at 1200 UTC for the tracers emitted at Passy, Sallanches and Chamonix (cf. Figure 8d–f). Their spatial distribution suggests that tracers are mainly extracted from the $BASIN_{low}$ volume by anabatic winds developed along the sunlit south-facing basin sidewalls (Figure 3b). In addition, the temporal evolution of the temperature structure has been analysed in an on-going study which shows that the daytime convective-layer thickness never exceeded 500 m during the stagnation stage of IOP1 (Y. Largeron, personal communication, 2019). This means that tracer transfer toward the ABO1500 volume can only be driven by along-slope flows.
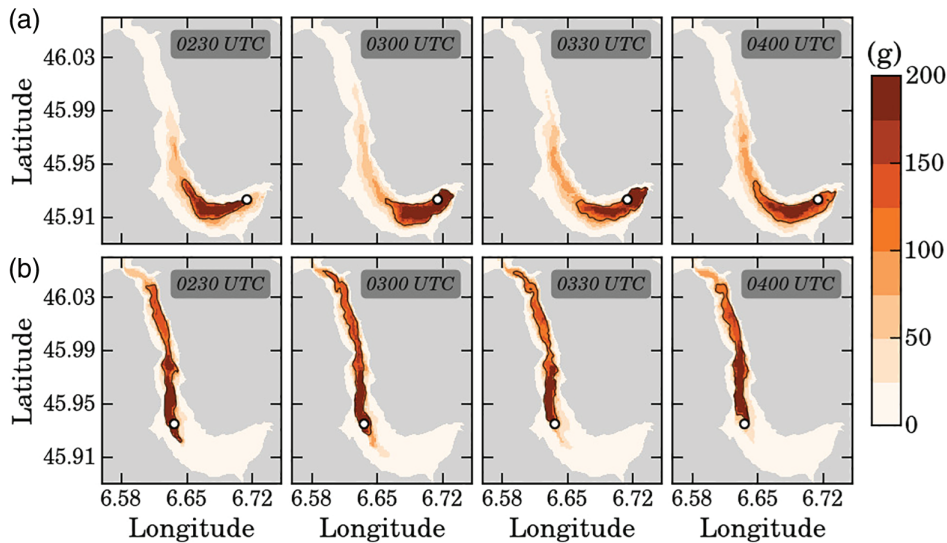
FIGURE 7 Night-time tracer plume evolution determined every 30 min between 0230 and 0400 UTC over the first 200 m above the ground for tracers emitted at (a) Passy and (b) Sallanches in the reference simulation. The emission sources are shown as white dots, and the 100 g iso-contours are shown in black
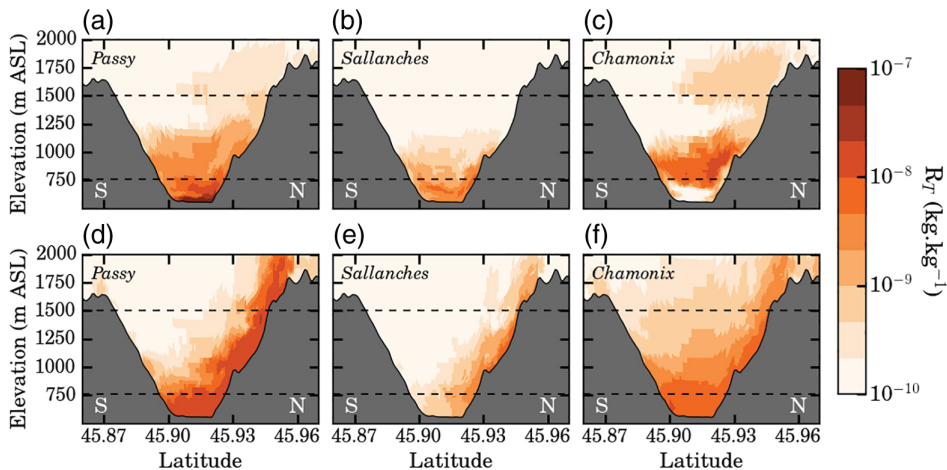

FIGURE 8 South–north cross-sections of tracer mixing ratio extracted in the the basin centre at (a–c) 0000 UTC and (d–f) 1200 UTC during the second day of the reference simulation for tracers emitted at (a, d) Passy, (b,e) Sallanches and (c, f) Chamonix. The horizontal dashed lines represent the intermediate and upper elevation thresholds used to mark out the three sub-volumes of the BASIN domain

The daytime export of Sallanches tracers out of the $BASIN_{low}$ volume appears less effective with a minimum mass of 9.7% reached at 1530 UTC while the Passy tracer mass goes below 4% at 1630 UTC (Figure 6b). This less effective evacuation is partly explained by a lower vertical transport with a maximum of 35% of mass transferred toward the ABO1500 volume for Sallanches tracers against 55% for Passy tracers. This difference emerges from a higher radiative warming of the south-facing sidewalls surrounding the Passy tracers source which favours the development of stronger anabatic winds (Part I). In comparison, the east-facing sidewalls near Sallanches are less exposed to daytime short-wave radiation. This result is illustrated by Figure 9 which represents horizontal cross-sections of mixing ratio extracted at 1,250 m asl for the two emission sources at 1200 UTC. At that time, the tracers emitted at Passy are mainly evacuated along the northeast sidewalls while Sallanches tracers mainly run along the western sidewalls of the basin. Later in the afternoon, the western sidewall goes into shadow while the south-facing slopes

are still illuminated; this permits a longer vertical transfer of the Passy tracers (not shown). Finally, the vertical tracer pumping efficiency depends on the exact location within the basin due to small-scale topographical features. This mechanism therefore induces a spatially heterogeneous tracer distribution at the basin scale.

In addition to a more effective vertical pumping, a small fraction of the Passy tracers is also vented out toward the $EAST_{low+interm}$ domain which contains 6% of the mass at 1530 UTC, as shown in Figure 6a. This upstream transport mechanism does not affect the Sallanches tracers which never exceed 0.3% of mass in the $EAST_{low+interm}$ domain. This result, combined with the absence of tracer in the SOUTH domain, highlights a very weak transfer of material from the basin toward the three surrounding tributary valleys during the daytime period. Consequently, the up-valley wind systems developed within these valleys have a poor ability to induce tracer displacement, while the mass budget computed in Part I has shown that they export more than half of the total basin
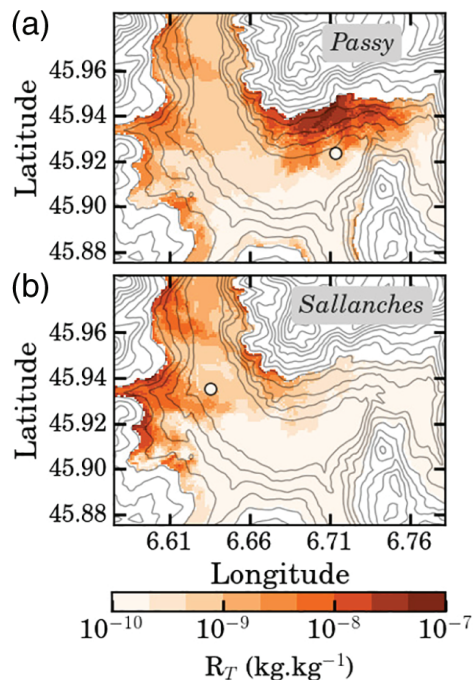
FIGURE 9 Horizontal cross-sections at 1250 m asl of mixing ratio at 1200 UTC for tracers emitted at (a) Passy and (b) Sallanches in the reference simulation. The emission sources are indicated by white dots

airmass (36.7×10^9, 8.6×10^9 and 16.8×10^9 kg of air through the Megève, Saint-Gervais and Chamonix valleys, respectively). This weak efficiency results from the establishment in two stages of (a) the along-slope circulation, which induces an exponential decrease of the mass in BASIN$_{low}$ volume, followed two hours later by (b) the up-valley wind system which is less efficient to ventilate the restricted near-surface volume in which tracers accumulate.

This first analysis finally shows that, during the daytime period, the vertical transport largely prevails over upstream transport for tracers emitted within the basin. As a consequence, the surrounding tributary valleys are isolated from the pollution accumulated within the basin. Rather, we showed that the tracers affect the south-facing basin sidewalls due to asymmetric thermal forcing, even at relatively high elevation (up to 2000 m asl) while pollutants have been emitted at 560 m asl. Similar dynamics have already been observed in the Austrian Inn Valley during a wintertime pollution episode (Gohm *et al.*, 2009; Harnisch *et al.*, 2009) and should be considered carefully since it may influence the atmospheric composition measured at high-altitude stations (Bukowiecki *et al.*, 2016; Hulin *et al.*, 2019). At night, the downstream transport appears as a second effective mechanism of material transport, but it mainly concerns the Sallanches tracers while Passy tracers tend to accumulate within the central curved sector of the BASIN$_{low}$ volume.

4.2.2 | Tracers emitted in the Chamonix valley

The time evolution of the mass distribution by sub-volumes for tracers emitted at Chamonix is presented in Figure 6c. In the framework of a constant emission rate, the mass maximum within the emission volume (EAST$_{low}$) occurs in the early evening of the first day with 43% of the tracer mass at 2030 UTC. Then, a negative slope (-2% hr^{-1} on average between 2100 and 0900 UTC) is observed in the EAST$_{low}$ volume which indicates an export of material exceeding the tracer accumulation. This tracer export is directed toward the basin where it mainly affects the intermediate volume with 37% of mass in BASIN$_{interm}$ at 0900 UTC of day 2 while only 7% has reached BASIN$_{low}$. This mass distribution is illustrated in Figure 8c representing the 0000 UTC south–north cross-section of Chamonix tracer mixing ratio in the basin centre. The position of the mixing ratio core corresponds with the down-valley wind structure displayed in figure 10 of Part I and points out the jet inability to plunge toward the lowest stratified layer of the basin atmosphere. The 7% of tracer mass observed in the BASIN$_{low}$ volume at 0900 UTC results from (a) a slight incorporation of material by katabatic winds and (b) the volume decomposition with the 760 m asl intermediate boundary crossing the jet structure, as can be seen in Figure 8c. Consequently, the tracers emitted within the Chamonix valley cannot be considered as a major contributor to the pollutant accumulation measured at the basin bottom during the night. The same conclusion is valid for the two southern tributary valleys whose associated down-valley winds also do not reach the basin bottom and flow at altitude as showed in Part I. This result was checked with an additional simulation in which tracer sources were initialized in the Megève and Saint-Gervais valleys and the associated tracer plumes were also observed at altitude during the night (not shown). Mid-altitude villages in the basin appear more impacted by pollutants from Chamonix and tributary valleys than villages located in the basin bottom.

In the early morning (0900 UTC of day 2), the Chamonix tracer mass is more important in the BASIN$_{interm}$ volume than in the EAST$_{low}$ volume of emission (37 versus 17% respectively), highlighting a higher ventilation of the Chamonix valley than of the basin (Figure 6c). Then, a mass decrease is observed in the BASIN$_{interm}$ volume between 0930 and 1600 UTC leading to a minimum mass of 9.8%. This diminution can be due to several mechanisms since the Chamonix tracers present in the basin intermediate volume after sunrise can be (a) incorporated within BASIN$_{low}$ by convective mixing, (b) vertically vented out by anabatic winds or (c) sent back toward the Chamonix valley by the up-valley wind system. Figure 8f shows that
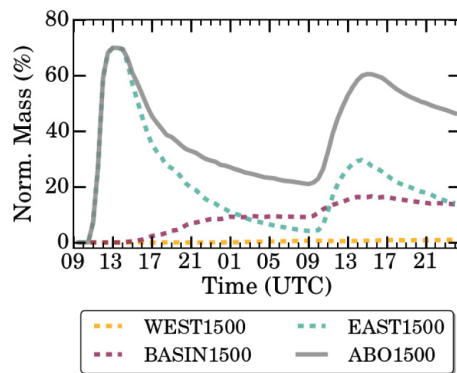
FIGURE 10 Temporal evolution from the reference simulation of the normalized Chamonix tracer mass in the ABO1500 volume and in the three upper (above 1,500 m asl) sub-volumes whose horizontal limits correspond to the BASIN, WEST and EAST domains shown in Figure 1a

convection allows an homogenization of the Chamonix mixing ratio in the BASIN$_{low}$ volume at 1200 UTC of day 2. However, the corresponding mass tracer in this lower volume never exceeds 8% (Figure 6c), indicating that the tracer transport is driven by the other mentioned mechanisms. Figure 6c shows that the tracer transfer is mainly directed toward the ABO1500 volume which contains 60% of the total Chamonix tracer mass at 1500 UTC of day 2. This vertical transport occurs both within the basin and the Chamonix valley as can been seen in Figure 10. This Figure represents the Chamonix tracer mass within three sub-volumes above 1,500 m asl (BASIN1500, WEST1500 and EAST1500) whose horizontal limits correspond to those of the BASIN, WEST and EAST domains (Figure 1a). Figure 10 shows that between 0900 and 1500 UTC of day 2, the mass in the BASIN1500 volume only increases from 9 to 17%, which is not enough to explain the mass diminution observed in the BASIN$_{interm}$ volume. Actually, a two-step mechanism develops with a first transfer from the BASIN back toward the EAST domain, quickly followed by a vertical export toward the EAST1500 volume by anabatic winds. The cleaning of BASIN$_{interm}$ volume therefore results from the combination of this two-step mechanism and the anabatic winds developed along the northern basin sidewalls, as illustrated in Figure 8f.

To summarize, the night-time accumulation of Chamonix tracers within the Chamonix valley is weak since they are efficiently advected by the down-valley flow toward the intermediate layer of the basin where they remain trapped. As a result, pollutants emitted at Chamonix do not participate in the pollution accumulation measured at the basin bottom. The same conclusion holds for pollutants emitted in the Megève and Saint-Gervais tributary valleys located in the SOUTH

domain. As a consequence, the tracer accumulation within the BASIN$_{low}$ volume presented in Figure 5 is only due to emissions intrinsic to the basin. In addition, the down-valley flows developed within the three tributary valleys cannot be considered as sources of ventilation which would explain the midnight drop in PM10 concentrations (Figure 2), as suggested by Chemel *et al.* (2016). On the contrary, they may influence the air quality of mid-altitude villages lying along the basin sidewalls. The nocturnally trapped and the diurnally emitted tracers are then lifted above 1,500 m asl by anabatic winds during daytime.

5 | PROCESS ANALYSIS AND IMPACT ON TRANSPORT MECHANISMS

The analysis proposed in the previous section for the reference simulation has also been performed for the set of numerical experiments described in Table 2. The aim is to quantify to what extent the tracer transport is modified in response to wind evolution induced by weaker initial stratification, higher radiative forcing or snow cover. For all the simulations, the mass distribution per sub-volume shows a temporal trend similar to REF (Figure 6), but with variations in the minimum and maximum percentages (not shown). The process analysis is therefore based on the average, maximum and minimum of normalized tracer masses determined over the second day of each simulation in the seven sub-volumes for the three emission sources. These values are reported in Figure 11 with one panel per tracer source. As for the reference simulation, the tracer masses in the SOUTH$_{low}$ and SOUTH$_{interm}$ volumes never exceed 1.5%, which is why these volumes are not represented.

For Passy tracers, the main evolution in mass distribution between the five simulations concerns the BASIN$_{low+interm}$ domain and the ABO1500 volume. The same volumes are concerned for Sallanches tracers which also show variations in the WEST$_{low+interm}$ domain. For Chamonix tracers, the variations mainly concern the BASIN$_{interm}$, EAST$_{low}$ and ABO1500 volumes. If the mass in the BASIN$_{interm}$ volume appears systematically higher than in the EAST$_{low}$ volume of emission, the tracer mass transferred toward the BASIN$_{low}$ volume never exceeds 8.5%. This means that for all the tested configurations, the tracers emitted in the Chamonix valley have a minor contribution to the tracer accumulated in the BASIN$_{low}$ atmosphere.

In the following, a focus is proposed on the processes influencing the transfer of tracers emitted within the basin (i.e., at Passy and Sallanches) by combining Figure 11 with

FIGURE 11 Average (dots), maximum and minimum (crosses) of normalized tracer masses determined in every sub-volume during the second day of the five simulations for tracers emitted at (a) Passy, (b) Sallanches and (c) Chamonix
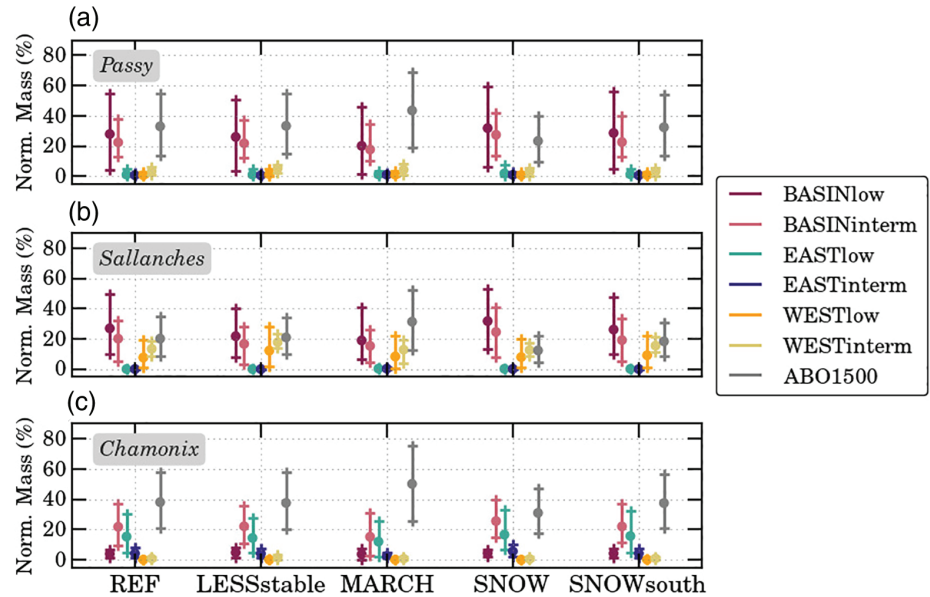

TABLE 3 Vertical, downstream and upstream transport efficiencies (expressed in %) determined for Passy and Sallanches tracers in each simulation

	Vertical transport		Downstream transport		Upstream transport	
	Passy	**Sallanches**	**Passy**	**Sallanches**	**Passy**	**Sallanches**
REF	54.9 (1530)	34.5 (1530)	8.9 (0900)	35.4 (0730)	6.3 (1530)	0.2 (1600)
LESSstable	54.4 (1530)	33.9 (1530)	12.7 (0900)	46.2 (0800)	6.5 (1530)	0.6 (1600)
MARCH	69.0 (1600)	52.3 (1530)	11.8 (0800)	40.3 (0800)	5.6 (1700)	2.5 (1700)
SNOW	40.2 (1600)	21.8 (1600)	7.8 (0930)	34.2 (0930)	10.2 (1530)	0.8 (1630)
SNOWsouth	53.7 (1530)	31.0 (1600)	8.2 (0900)	38.9 (0800)	6.4 (1530)	0.3 (1530)

TABLE 4 Normalized tracer mass (expressed in %) within the $BASIN_{low}$ volume at 0800 and 1600 UTC of day 2 for Passy and Sallanches tracers in each simulation

	0800 UTC		1600 UTC	
	Passy	**Sallanches**	**Passy**	**Sallanches**
REF	54.4	42.3	4.1	10.1
LESSstable	50.0	32.3	3.5	8.7
MARCH	45.7	32.4	1.8	6.7
SNOW	59.0	44.4	6.2	14.0
SNOWsouth	55.5	37.2	4.6	10.0

Tables 3 and 4. Table 3 aims to compare the efficiency of the three mechanisms of tracer transport defined in Section 3.3 (vertical, downstream, upstream). The quantification of the mechanism efficiency is determined as the maximum of normalized tracer mass in the:

- $ABO1500$ volume for vertical transport,
- $WEST_{low+interm}$ volumes for downstream transport,
- $EAST_{low+interm}$ volumes for upstream transport.

These percentages are reported in Table 3 for Passy and Sallanches tracers along with the corresponding times which vary in response to wind circulation evolution described in Part I. The determination of tracer accumulation within the $BASIN_{low}$ volume is proposed by comparison with Table 4 which gathers the normalized mass of Passy and Sallanches tracers in the $BASIN_{low}$ volume at 0800 and 1600 UTC of the second day of simulation. Those hours are chosen in order (a) to quantify the night-time accumulation and daytime ventilation of the $BASIN_{low}$ volume and (b) to account for the daytime regime lengthening under the early-spring radiative forcing.

5.1 | Vertical transport by anabatic winds

We have seen in Section 4.2.1 that in the reference simulation, the vertical transport by anabatic winds toward

the ABO1500 volume is more effective for Passy than Sallanches tracers with respective mass maximum of 54.9 and 34.5% reached at 1530 UTC, representing a Passy/Slchs ratio of 1.6. A similar trend is observed for all the simulations with a ratio ranging from 1.3 to 1.8. The smallest difference concerns the MARCH simulation with a maximum of 69% of mass in the ABO1500 volume for Passy and 52.3% for Sallanches (Table 3). This result is in agreement with the along-slope circulation evolution discussed in Part I with a lengthening of the anabatic regime that develops over a wider area. This augmentation of vertical export directly impacts the masses remaining in the BASIN$_{low}$ volume which become lower than 2 and 7% for Passy and Sallanches tracers respectively at 1600 UTC (Table 4). In addition, the more developed convective boundary layer allows a more effective cleaning of the BASIN$_{interm}$ volume but it does not participate in the transfer toward ABO1500 since it never exceeds 1,300 m asl (not shown). As a result, the radiative forcing in March allows an overall cleaning of the atmosphere below 1,500,m asl, as can be seen in Figure 11 with an increase of average, minimum and maximum masses in the ABO1500 volume which corresponds to an overall mass diminution in the six other sub-volumes for the three emission sources. This result is in line with the conclusion of Leukauf *et al.* (2016) who showed a more effective tracer export out of their idealized valley under higher solar forcing conditions.

On the contrary, a general mass increase occurs in the volumes below 1,500 m asl in the SNOW simulation because of a less effective vertical transport of tracer (Figure 11). Table 3 shows a diminution of the tracer mass in the ABO1500 volume of 14.7 and 12.7 units for Passy and Sallanches tracers respectively in comparison with REF. This evolution is in line with the literature (Chazette *et al.*, 2005; Lehner and Gohm, 2010; Whiteman *et al.*, 2014) and with the weakening of anabatic winds under snow-covered conditions discussed in Part I. The impact of the snow cover state investigated through the SNOWsouth simulation does not show a marked variation in comparison with REF. Nevertheless, a more detailed study of this simulation will be proposed in section 5.4 so as to analyse the tracer plume behaviour in response to the snow cover state.

Last, in the LESSstable simulation, the vertical transport efficiency remains close to the reference case, meaning that, contrary to other studies (Lehner and Gohm, 2010; Leukauf *et al.*, 2015), the initial temperature profile does not represent a critical parameter for the vertical pumping of tracers by anabatic winds in our configuration. This weak influence may be related to the relatively small difference in initial stability between LESSstable and REF since vertical temperature profiles converge in the morning of the second day of simulation (not shown).

5.2 | Downstream transport

The downstream transport appears systematically more effective for Sallanches than Passy tracers with a mass transfer from the BASIN toward the WEST domain which is at least 3.4 times higher for Sallanches tracers (Table 3).

The most efficient export of Sallanches tracers concerns the LESSstable simulation with 46.2% of the mass in the WEST domain at 0800 UTC representing an augmentation of 10.8 units with respect to REF. This augmentation is associated with a diminution from 42.3% in REF to 32.3% in LESSstable of the Sallanches tracers accumulated within the BASIN$_{low}$ volume at 0800 UTC (Table 4). This diminution is in agreement with the wind dynamics evolution discussed in Part I with an intensification of the near-surface down-valley flow in the western linear part of the basin. This means that the initial thermal stability does play a role in the efficiency of the night-time transport of pollutant, with an increased thermal stability tending to inhibit the down-valley wind system and the associated ventilation.

In MARCH, the masses accumulated in the BASIN$_{low}$ volume at 0800 UTC appear less important for both emission sources, as shown by Table 4. This diminution results from the combination of (a) a more effective downstream transport developed at night (plus 5 and 3 units for Sallanches and Passy respectively) and (b) a more efficient vertical pumping of tracers which permits a cleaning of the basin atmosphere during the daytime period, as discussed in the previous section. On the contrary, the higher tracer accumulation within the BASIN$_{low}$ volume in the SNOW simulation (59% at 0800 UTC) results from the combination of a slightly less effective downstream transport and a lower vertical pumping by anabatic winds.

5.3 | Upstream transport

The upstream transport does not show marked evolutions between the five simulations, as shown in Table 3. Moreover, this mechanism appears as the least effective for tracer transfer since it never affects more than 10.2% of the tracer mass. As discussed for the reference simulation, the upstream transport mainly concerns the Passy tracers because of the source proximity with the EAST domain. The highest augmentation occurs in the SNOW simulation with 10.2% of the Passy tracer mass transferred toward the EAST domain, instead of 6.3% in REF. This increase results from a less effective cleaning of the basin atmosphere by vertical pumping because of the weakening of the anabatic winds. It therefore illustrates that, when the main transport mechanism becomes less efficient, secondary mechanisms become of greater relative
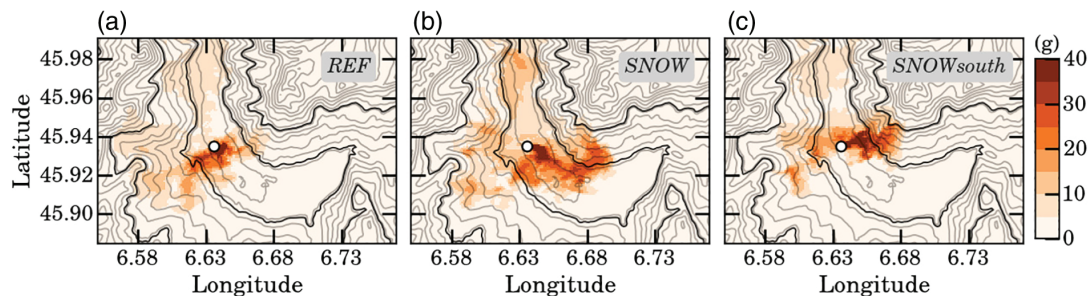
FIGURE 12 Mass of tracer emitted at Sallanches, computed in the first 30 m above the ground at 1230 UTC for simulations (a) REF, (b) SNOW and (c) SNOWsouth. The darkest contours represent the 760 m asl and 1,500 m asl elevation thresholds used to define the basin volumes. The white dot indicates the Sallanches tracer source

importance. Under the radiative forcing of March, the upstream transport becomes less effective than in the REF simulation with only 5.6% of Passy tracers transferred toward the EAST domain. This means that the intensification of the up-valley wind within the basin and the increase of the flux toward the Chamonix valley discussed in Part I do not favour the tracer transfer toward this valley, as could be expected. This absence of transfer finally confirms that the up-valley wind systems do not represent an effective mechanism for cleaning the near-surface atmosphere, even under the most favourable configuration tested in the present study. Rather, the tracer export is driven by anabatic winds probably because of their earlier establishment, their lower inertia and their proximity with the surface which facilitates the pumping of the near-surface atmosphere where night-time pollution accumulates.

5.4 | Impact of snow cover

The simulation SNOWsouth addresses the question of the influence of a snow cover restricted to the north-facing shaded slopes of the basin (Table 2). Under these conditions, Figure 11 and Table 3 suggest that the tracer distribution per sub-volume and the transport mechanism efficiencies do not change a lot in comparison with the reference simulation. However, the spatial evolution of the plume does evolve generating local heterogeneities between snow-covered and snow-free slopes, in particular for Sallanches tracers. This result is illustrated in Figure 12 which represents the Sallanches tracer plume, expressed in mass of tracers within the first 30 m above the ground at 1230 UTC for simulations REF, SNOW and SNOWsouth.

In the reference simulation (Figure 12a), the tracers emitted at Sallanches are efficiently vertically vented out by anabatic winds which first develop along the western slopes as shown in Figure 9b, leading to dilution of the plume in the lowest basin atmosphere. When a snow cover is present over the entire domain (SNOW), a more marked

plume is observed in the lowest atmospheric levels of the basin because of the less effective vertical pumping by anabatic winds which reduces the material extraction (Figure 12b). In the SNOWsouth situation (Figure 12c), the plume is directed toward the northern slopes of the basin where anabatic winds are well established. Since the vertical transport which should occur in a first place along the western slopes is reduced because of the snow, the northern sidewall of the basin becomes more affected by pollution. This result is not accessible directly from Tables 3 and 4 since at 1600 UTC, the Sallanches tracer mass remaining in the $BASIN_{low}$ volume is similar in REF and SNOWsouth (10.1 and 10% respectively). However this complementary analysis of the plume demonstrates that the tracers are well extracted in both situations but are not evacuated along the same sidewalls in response to the spatial re-organization of the most effective transport mechanisms.

6 | DISCUSSION

The present study falls between idealized (e.g. Lehner and Gohm, 2010; Lang *et al.*, 2015; Leukauf *et al.* 2016; Quimbayo-Duarte *et al.*, 2019) and real-case (e.g., Martínez *et al.*, 2010; Jiménez and Cuxart, 2014; Jiménez *et al.*, 2019) studies as we consider a realistic orography and a simplified initialization of the atmosphere. The use of a realistic orography is necessary as it greatly modulates local thermally driven flows (Rucker *et al.*, 2008; Duine *et al.*, 2017). The simplified atmospheric state (initial zero wind profile, no large-scale tendency) has the advantage of focusing on tracer dispersion by local circulations without considering large-scale coupling. The decoupling between local and large-scale circulations is often assumed under wintertime anticyclonic situations (Schäfer *et al.*, 2008; Reeves and Stensrud, 2009), although the local dynamics could be modulated by the large-scale flow. In the future, an opportunity could be taken to add a large-scale

wind to the current numerical configuration in order to investigate its impact on local circulations. The use of passive tracers emitted continuously at a constant rate at three locations permits comparison of how the tracers are transported depending on their source location within the valley. This approach allows us to affirm that the local wind dynamics participate in the pollution heterogeneity observed over the area, which is therefore not solely due to emission features as the study does not rely on an emission inventory. More precisely, the following results are in line with the observed pollution features highlighted in Figure 2 :

- The Chamonix valley is less polluted than the basin due to (a) a more effective night-time tracer transport induced by a more intense down-valley flow and (b) a lack of daytime tracer advection from the basin since the pollution has already been vertically evacuated by anabatic winds.
- The central curved part of the basin (around Passy) is more favourable to night-time pollutant accumulation since it is subject to wind oscillations and a re-circulation cell which favour the airmass stagnation. On the contrary, the more established down-valley wind developed in the western linear part of the basin (around Sallanches) allows a more effective evacuation of pollutants emitted at Sallanches than those released at Passy.

These results also show that, despite its central position within the valley, the basin cannot be considered as a pollution repository as its near-surface atmosphere remains almost unaffected by the night-time pollution from the surrounding tributary valleys.

The present work finally highlights the importance of model high resolution to adequately represent the fine-scale circulations which significantly differ from one valley to another and play a major role in pollutant dispersion. Furthermore, the snow cover state appears as an important factor in tracer dispersion, as shown by the comparison of SNOW and SNOWsouth simulations (Figure 12). This means that a proper initialization of the snow cover is also required at high resolution to ensure accurate air quality forecasting and to identify the most vulnerable areas. This conclusion is in line with Chow *et al.* (2006), Tomasi *et al.* (2017) and Lehner and Rotach (2018) who all recommend an overall improvement of the land cover initialization. Note that the present numerical set-up could be used again to quantify the tracer plume sensitivity to surface properties such as soil moisture, which is known to modulate the slope-circulation through the surface energy budget (Chow *et al.*, 2006; Rihani *et al.*, 2015) or land-use resolution (Schicker *et al.* 2016).

Starting from these results, a deeper understanding of the diurnal evolution of PM10 concentrations could now be achieved by cross-referencing these wind dynamics with more realistic space- and time-varying emissions (either at some point sources or in the entire area). Actually a full understanding of the hourly PM concentrations presented in Figure 2 would require a complete and accurate emission inventory (including realistic spatio-temporal structure) combined with complete and accurate simulations of the wind structure.

7 | CONCLUSIONS

The present study addresses the question of the influence of wind dynamics on pollutant dispersion in a part of the Alpine Arve River valley using a set of high-resolution numerical simulations. This area includes a constricted basin which frequently suffers from severe wintertime PM10 pollution episodes while the surrounding tributary valleys appear to be significantly less affected. A tracer tracking is performed by dividing the atmosphere into near-surface, intermediate and upper volumes for each valley within the area. Passive tracers are emitted continuously at a constant rate at three point sources – two within the basin (Passy and Sallanches) and one in the tributary Chamonix valley. This approach allows us to determine to what extent local flows drive the transfer of tracers within a given valley from one layer to another and also between the different valleys. This methodology is applied over

(i) a reference simulation representative of a wintertime local pollution event based on conditions encountered during the IOP1 of the Passy-2015 field experiment, and

(ii) a set of numerical experiments designed to quantify the tracer transport evolution under less stable conditions, higher radiative forcing and snow cover situations.

The following conclusions are drawn in response to the questions introduced at the beginning of the study.

- *Among the characteristics of the dynamics described in Part I, which ones play a major role in tracer transport? What is the relative influence of the along-slope and along-valley circulations?*

During daytime, the vertical transport by anabatic winds largely prevails over the horizontal transport by up-valley wind. This results from an earlier establishment of anabatic winds which develop near the ground thereby favouring an efficient pumping of the near-surface atmosphere in which tracers accumulate. This mechanism permits the transfer of material toward the upper atmospheric volume and considerably reduces the near-surface accumulation.

This mechanism is also responsible for a basin-scale heterogeneous pollution field as tracers are mainly evacuated along the sunlit sidewalls. At night, the horizontal transport associated with the down-valley wind represents another effective transport mechanism for tracers emitted within the basin. However, this mechanism appears more effective in the western linear part (Sallanches) than in the central curved part (Passy) of the basin because of unequally developed near-surface flows, as shown in Part I. The efficiency of the transport mechanisms can finally be classified as follows: the vertical transport prevails over downstream transport, which prevails over upstream transport. This conclusion cannot be directly extrapolated to other Alpine valleys since it strongly depends on local orographic arrangement. However, it highlights the necessity for a fine-resolution model and orography to ensure accurate pollution forecasting over mountainous terrains.

- *How are the tracers distributed between the atmospheric volumes within the valleys dependent on the emission source location? More precisely, to what extent are the tracers emitted (a) in the Chamonix valley incorporated within the basin, and (b) within the basin evacuated toward the tributary valleys?*

- During daytime, tracers are mainly evacuated by anabatic winds toward the upper valley atmosphere, meaning that they do not affect the surrounding tributary valleys. During night-time, a fraction of the tracers emitted within the basin is exported toward the downstream part of the valley while the rest accumulates within its emission volume (which contains 55 and 44% of the tracer mass at the end of the night for Passy and Sallanches tracers, respectively). On the other hand, tracers emitted within the upstream Chamonix valley are efficiently evacuated toward the basin at night due to a more effective night-time ventilation by the down-valley wind leading to a weak accumulation within their emission volume (only 20% at the end of the night). However, we have shown that the Chamonix tracers do not participate in the night-time accumulation measured at the near-surface basin because of the down-valley wind not reaching the stratified near-surface atmosphere. Rather, those tracers accumulate within the intermediate atmospheric volume of the basin. This result can be generalized to the tracers emitted within the other tributary valleys, as the associated drainage flows also do not reach the near-surface stratified basin atmosphere. Consequently, the near-surface basin atmosphere cannot be considered as a receptacle for pollution emitted in the surrounding valleys at night. Rather, this pollution is likely to degrade the air quality of mid-altitude villages lying along the basin sidewalls.

- *What role do the early-spring solar forcing (March), the initial stability and the snow cover play in the trapping of pollutants within the near-surface atmosphere?*

At the slope scale, the tracer transport by anabatic winds becomes more effective under the radiative forcing of March (69% and 55% of Passy tracers are advected toward the upper atmosphere in March and February respectively). However, this vertical transport becomes less effective under snow cover situations (with only 40% of Passy tracers advected toward the upper atmosphere), thereby increasing the tracer accumulation in the near-surface atmosphere. The snow cover state also appears as an important feature by modulating the tracer plume orientation. At the valley scale, the horizontal transport by down-valley wind becomes more effective as the thermal stability decreases, thereby reducing the tracer accumulation within the basin in the morning.

Our simplified approach finally brings new insights into the tracer transport mechanisms developed within this highly complex terrain; these mechanisms are consistent with the PM10 accumulation measured within the basin and may give rise to the basin-scale heterogeneous pollution field. A deeper understanding of the PM10 concentration time cycle would now require a more realistic initialization of emission sources and the use of on-line chemistry in order to combine the atmospheric dynamics with the spatio-temporal evolution of pollutants.

CONFLICT OF INTEREST

The authors declare no conflict of interest.

ORCID

Tiphaine Sabatier https://orcid.org/0000-0001-8489-6331

REFERENCES

Adler, B. and Kalthoff, N. (2014) Multi-scale transport processes observed in the boundary layer over a mountainous island. *Boundary-Layer Meteorology*, 153, 515–537

Allwine, K.J. and Whiteman, C.D. (1994) Single-station integral measures of atmospheric stagnation, recirculation and ventilation. *Atmospheric Environment*, 28, 713–721

Atmo-AURA (2016). *Bilan de la qualité de l'air 2015 – rapport annuel.* Atmo-Auvergne Rhônes-Alpes. Technical Report. Available at: https:// www.atmo-auvergnerhonealpes.fr/publications/diagnostic-annuel-bilan-de-la-qualite-de-lair-2015-region-rhone-alpes; accessed 24 November 2019.

Bader, D.C. and Whiteman, C.D. (1989) Numerical simulation of cross-valley plume dispersion during the morning transition period. *Journal of Applied Meteorology*, 28, 652–664

Bukowiecki, N., Weingartner, E., Gysel, M., Coen, M.C., Zieger, P., Herrmann, E., Steinbacher, M., Gäggeler, H.W. and Baltensperger, U. (2016) A review of more than 20 years of aerosol observation at the high altitude research station Jungfraujoch, Switzerland (3580 m asl). *Aerosol and Air Quality Research*, 16, 764–788

Chazette, P., Couvert, P., Randriamiarisoa, H., Sanak, J., Bonsang, B., Moral, P., Berthier, S., Salanave, S. and Toussaint, F. (2005) Three-dimensional survey of pollution during winter in French Alps valleys. *Atmospheric Environment*, 39, 1035–1047

Chemel, C., Arduini, G., Staquet, C., Largeron, Y., Legain, D., Tzanos, D. and Paci, A. (2016) Valley heat deficit as a bulk measure of wintertime particulate air pollution in the Arve River valley. *Atmospheric Environment*, 128, 208–215

Chow, F.K., Weigel, A.P., Street, R.L., Rotach, M.W. and Xue, M. (2006) High-resolution large-eddy simulations of flow in a steep Alpine valley. Part I: methodology, verification, and sensitivity experiments. *Journal of Applied Meteorology and Climatology*, 45, 63–86

Colella, P. and Woodward, P.R. (1984) The piecewise parabolic method (PPM) for gas-dynamical simulations. *Journal of Computational Physics*, 54, 174–201

Cuxart, J., Bougeault, P. and Redelsperger, J.-L. (2000) A turbulence scheme allowing for mesoscale and large-eddy simulations. *Quarterly Journal of the Royal Meteorological Society*, 126, 1–30

Deardorff, J.W. (1974) Three-dimensional numerical study of turbulence in an entraining mixed layer. *Boundary-Layer Meteorology*, 7, 199–226

Defant, F. (1949). A theory of slope winds, along with remarks on the theory of mountain winds and valley winds, *Alpine Meteorology*. Richland, WA: F. PNL-5141/ASCOT-84-3, Pacific Northwest Laboratory.

Diémoz, H., Barnaba, F., Magri, T., Pession, G., Dionisi, D., Pittavino, S., Tombolato, I.K.F., Campanelli, M., Della Ceca, L.S., Hervo, M., Di Liberto, L., Ferrero, L. and Gobbi, G.P. (2019) Transport of Po valley aerosol pollution to the northwestern Alps – Part 1: phenomenology. *Atmospheric Chemistry and Physics*, 19, 3065–3095. https://doi.org/10.5194/acp-19-3065-2019

Duine, G.-J., Hedde, T., Roubin, P., Durand, P., Lothon, M., Lohou, F., Augustin, P. and Fourmentin, M. (2017) Characterization of valley flows within two confluent valleys under stable conditions: observations from the KASCADE field experiment. *Quarterly Journal of the Royal Meteorological Society*, 143, 1886–1902

Faroux, S., Kaptué Tchuenté, A.T., Roujean, J.-L., Masson, V., Martin, E. and Le Moigne, P. (2013) ECOCLIMAP-II/Europe: a twofold database of ecosystems and surface parameters at 1 km resolution based on satellite information for use in land surface, meteorological and climate models. *Geoscientific Model Development*, 6, 563–582. https://doi.org/10.5194/gmd-6-563-2013

Fouquart, Y. and Bonnel, B. (1980) Computations of solar heating of the Earth's atmosphere – a new parameterization. *Beitr'age zur Physik der Atmosph'are*, 53, 35–62

Gal-Chen, T. and Somerville, R.C. (1975) Numerical solution of the Navier–Stokes equations with topography. *Journal of Computational Physics*, 17, 276–310

Gohm, A., Harnisch, F. and Fix, A. (2006). Boundary-layer structure in the Inn valley during high air pollution (INNAP). Extended abstract in Proceedings of the 12th AMS Conference on Mountain Meteorology, 28 August–1 September 2006, Santa Fe, NM. Available at: http://ams.confex.com/ams/pdfpapers/114458.pdf; accessed 24 November 2019.

Gohm, A., Harnisch, F., Vergeiner, J., Obleitner, F., Schnitzhofer, R., Hansel, A., Fix, A., Neininger, B., Emeis, S. and Schäfer, K. (2009) Air pollution transport in an Alpine valley: results from airborne and ground-based observations. *Boundary-Layer Meteorology*, 131, 441–463

Gudiksen, P.H. and Shearer, D.L. (1989) The dispersion of atmospheric tracers in nocturnal drainage flows. *Journal of Applied Meteorology*, 28, 602–608

Harnisch, F., Gohm, A., Fix, A., Schnitzhofer, R., Hansel, A. and Neininger, B. (2009) Spatial distribution of aerosols in the Inn valley atmosphere during wintertime. *Meteorology and Atmospheric Physics*, 103, 223–235

Henne, S., Furger, M., Nyeki, S., Steinbacher, M., Neininger, B., De Wekker, S., Dommen, J., Spichtinger, N., Stohl, A. and Prévôt, A. (2004) Quantification of topographic venting of boundary-layer air to the free troposphere. *Atmospheric Chemistry and Physics*, 4, 497–509

Hulin, M., Gheusi, F., Lothon, M., Pont, V., Lohou, F., Ramonet, M., Delmotte, M., Derrien, S., Athier, G., Meyerfeld, Y., Y. Bezombes., P. Augustin. and F. Ravetta. (2019) Observations of thermally driven circulations in the Pyrenees: comparison of detection methods and impact on atmospheric composition measured at a mountaintop. *Journal of Applied Meteorology and Climatology*, 58, 717–740. https://doi.org/10.1175/JAMC-D-17-0268.1

Jiménez, M.A. and Cuxart, J. (2014) A study of the nocturnal flows generated in the north side of the Pyrenees. *Atmospheric Research*, 145, 244–254

Jiménez, M.A., Cuxart, J. and Daniel, M.V. (2019) Influence of a valley exit jet on the nocturnal atmospheric boundary layer at the foothills of the Pyrenees. *Quarterly Journal of the Royal Meteorological Society*, 145, 356–375

Kalthoff, N., Horlacher, V., Corsmeier, U., Volz-Thomas, A., Kolahgar, B., Geiß, H., Möllmann-Coers, M. and Knaps, A. (2000) Influence of valley winds on transport and dispersion of airborne

pollutants in the Freiburg–Schauinsland area. *Journal of Geophysical Research*, 105, 1585–1597

Kukkonen, J., Pohjola, M., Sokhi, R.S., Luhana, L., Kitwiroon, N., Fragkou, L., Rantamäki, M., Berge, E., Ødegaard, V., Slørdal, L.H., Denby, B. and Finardi, S. (2005) Analysis and evaluation of selected local-scale PM10 air pollution episodes in four European cities: Helsinki, London, Milan and Oslo. *Atmospheric Environment*, 39, 2759–2773. https://doi.org/10.1016/j.atmosenv.2004.09.090

Lac, C., Chaboureau, J.-P., Masson, V., Pinty, J.-P., Tulet, P., Escobar, J., Leriche, M., Barthe, C., Aouizerats, B., Augros, C., Aumond, P., Auguste, F., Bechtold, P., Berthet, S., Bielli, S., Bosseur, F., Caumont, O., Cohard, J.-M., Colin, J., Couvreux, F., Cuxart, J., Delautier, G., Dauhut, T., Ducrocq, V., Filippi, J.-B., Gazen, D., Geoffroy, O., Gheusi, F., Honnert, R., Lafore, J.-P., Lebeaupin Brossier, C., Libois, Q., Lunet, T., Mari, C., Maric, T., Mascart, P., Mogé, M., Molinié, G., Nuissier, O., Pantillon, F., Peyrillé, P., Pergaud, J., Perraud, E., Pianezze, J., Redelsperger, J.-L., Ricard, D., Richard, E., Riette, S., Rodier, Q., Schoetter, R., Seyfried, L., Stein, J., Suhre, K., Taufour, M., Thouron, O., Turner, S., Verrelle, A., Vié, B., Visentin, F., Vionnet, V. and Wautelet, P. (2018) Overview of the Meso-NH model version 5.4 and its applications. *Geoscientific Model Development*, 11, 1929–1969. https://doi.org/10.5194/gmd-11-1929-2018

Lang, M.N., Gohm, A. and Wagner, J.S. (2015) The impact of embedded valleys on daytime pollution transport over a mountain range. *Atmospheric Chemistry and Physics*, 15, 11981–11998

Lareau, N.P., Crosman, E., Whiteman, C.D., Horel, J.D., Hoch, S.W., Brown, W.O. and Horst, T.W. (2013) The persistent cold-air pool study. *Bulletin of the American Meteorological Society*, 94, 51–63

Largeron, Y. and Staquet, C. (2016) Persistent inversion dynamics and wintertime PM_{10} air pollution in Alpine valleys. *Atmospheric Environment*, 135, 92–108

Lehner, M. and Gohm, A. (2010) Idealised simulations of daytime pollution transport in a steep valley and its sensitivity to thermal stratification and surface albedo. *Boundary-layer meteorology*, 134, 327–351

Lehner, M. and Rotach, M. (2018) Current challenges in understanding and predicting transport and exchange in the atmosphere over mountainous terrain. *Atmosphere*, 9, 276

Leukauf, D., Gohm, A., Rotach, M.W. and Wagner, J.S. (2015) The impact of the temperature inversion breakup on the exchange of heat and mass in an idealized valley: sensitivity to the radiative forcing. *Journal of Applied Meteorology and Climatology*, 54, 2199–2216

Leukauf, D., Gohm, A. and Rotach, M.W. (2016) Quantifying horizontal and vertical tracer mass fluxes in an idealized valley during daytime. *Atmospheric Chemistry and Physics*, 16, 13049–13066

Malek, E., Davis, T., Martin, R.S. and Silva, P.J. (2006) Meteorological and environmental aspects of one of the worst national air pollution episodes (January, 2004) in Logan, Cache Valley, Utah, USA. *Atmospheric Research*, 79, 108–122

Martínez, D., Jiménez, M., Cuxart, J. and Mahrt, L. (2010) Heterogeneous nocturnal cooling in a large basin under very stable conditions. *Boundary-Layer Meteorology*, 137, 97–113

Masson, V., Le Moigne, P., Martin, E., Faroux, S., Alias, A., Alkama, R., Belamari, S., Barbu, A., Boone, A., Bouyssel, F., Brousseau, P., Brun, E., Calvet, J.-C., Carrer, D., Decharme, B., Delire, C., Donier, S., Essaouini, K., Gibelin, A.-L., Giordani, H., Habets, F.,

Jidane, M., Kerdraon, G., Kourzeneva, E., Lafaysse, M., Lafont, S., Lebeaupin Brossier, C., Lemonsu, A., Mahfouf, J.-F., Marguinaud, P., Mokhtari, M., Morin, S., Pigeon, G., Salgado, R., Seity, Y., Taillefer, F., Tanguy, G., Tulet, P., Vincendon, B., Vionnet, V. and Voldoire, A. (2013) The SURFEXv7.2 land and ocean surface platform for coupled or offline simulation of earth surface variables and fluxes. *Geoscientific Model Development*, 6, 929–960. https://doi.org/10.5194/gmd-6-929-2013

Mlawer, E.J., Taubman, S.J., Brown, P.D., Iacono, M.J. and Clough, S.A. (1997) Radiative transfer for inhomogeneous atmospheres: RRTM, a validated correlated-k model for the longwave. *Journal of Geophysical Research*, 102, 16663–16682

O'Steen, L.B. (2000) Numerical simulation of nocturnal drainage flows in idealized valley–tributary systems. *Journal of Applied Meteorology*, 39, 1845–1860

Paci, A., Staquet, C., Allard, J., Barral, H., Canut, G., Cohard, J.-M., Jaffrezo, J.-L., Martinet, P., Sabatier, T., Troude, F., Arduini, G., Burnet, F., Brun, C., Chemel, C., Dabas, A., Donier, J.-M., Garrouste, O., Guillot, R., Largeron, Y., Legain, D., Maurel, W., Tzanos, D., Barrau, S., Barret, M., Barrie, J., Belleudy, A., Bouhours, G., Bourrianne, T., Chevrier, F., Douffet, T., Etcheberry, J.-M., Gustave, L., Mazoyer, M., Mercier, S., Moulin, E., Pellan, Y., Piguet, B., Rodier, Q. and Zin, I. (2016) The Passy-2015 Field Experiment: Atmospheric dynamics and air quality in the Arve River valley. *Pollution Atmosphérique*, 231–232. https://doi.org/10.4267/pollution-atmospherique.5903

Pardyjak, E.R., Fernando, H.J.S., Hunt, J.C.R., Grachev, A.A. and Anderson, J. (2009) A case study of the development of nocturnal slope flows in a wide open valley and associated air quality implications. *Meteorologische Zeitschrift*, 18, 85–100. https://doi.org/10.1127/0941-2948/2009/362

Pernigotti, D., Rossa, A.M., Ferrario, M.E., Sansone, M. and Benassi, A. (2007) Influence of ABL stability on the diurnal cycle of PM10 concentration: illustration of the potential of the new Veneto network of MW-radiometers and SODAR. *Meteorologische Zeitschrift*, 16, 505–511. https://doi.org/10.1127/0941-2948/2007/0204

Perrino, C., Catrambone, M., Dalla Torre, S., Rantica, E., Sargolini, T. and Canepari, S. (2014) Seasonal variations in the chemical composition of particulate matter: a case study in the Po valley. Part I: macro-components and mass closure. *Environmental Science and Pollution Research International*, 21, 3999–4009. https://doi.org/10.1007/s11356-013-2067-1

Quimbayo-Duarte, J., Staquet, C., Chemel, C. and Arduini, G. (2019) Impact of along-valley orographic variations on the dispersion of passive tracers in a stable atmosphere. *Atmosphere*, 10, 1–18. https://doi.org/10.3390/atmos10040225

Reeves, H.D. and Stensrud, D.J. (2009) Synoptic-scale flow and valley cold pool evolution in the western United States. *Weather and Forecasting*, 24, 1625–1643

Rendón, A.M., Salazar, J.F., Palacio, C.A. and Wirth, V. (2015) Temperature inversion breakup with impacts on air quality in urban valleys influenced by topographic shading. *Journal of Applied Meteorology and Climatology*, 54, 302–321

Ricard, D., Lac, C., Riette, S., Legrand, R. and Mary, A. (2013) Kinetic energy spectra characteristics of two convection-permitting limited-area models AROME and meso-NH. *Quarterly Journal of the Royal Meteorological Society*, 139, 1327–1341

Rihani, J.F., Chow, F.K. and Maxwell, R.M. (2015) Isolating effects of terrain and soil moisture heterogeneity on the atmospheric boundary layer: idealized simulations to diagnose land–atmosphere feedbacks. *Journal of Advances in Modeling Earth Systems*, 7, 915–937

Rotach, M.W., Wohlfahrt, G., Hansel, A., Reif, M., Wagner, J. and Gohm, A. (2014) The world is not flat: implications for the global carbon balance. *Bulletin of the American Meteorological Society*, 95, 1021–1028

Rucker, M., Banta, R.M. and Steyn, D.G. (2008) Along-valley structure of daytime thermally driven flows in the Wipp valley. *Journal of Applied Meteorology and Climatology*, 47, 733–751

Sabatier, T., Paci, A., Canut, G., Largeron, Y., Dabas, A., Donier, J.-M. and Douffet, T. (2018) Wintertime local wind dynamics from scanning Doppler lidar and air quality in the Arve River valley. *Atmosphere*, 9, 1–28. https://doi.org/10.3390/atmos9040118

Sabatier, T., Paci, A., Lac, C., Canut, G., Largeron, Y. and Masson, V. (2019) Semi-idealized simulations of wintertime flow and pollutant transport in an Alpine valley. Part I: Origins of local circulations. *Quarterly Journal of the Royal Meteorological Society*, ???

Schäfer, K., Vergeiner, J., Emeis, S., Wittig, J., Hoffmann, M., Obleitner, F. and Suppan, P. (2008) Atmospheric influences and local variability of air pollution close to a motorway in an alpine valley during winter. *Meteorologische Zeitschrift*, 17, 297–309

Schicker, I., Arias, D.A. and Seibert, P. (2016) Influences of updated land-use datasets on WRF simulations for two Austrian regions. *Meteorology and Atmospheric Physics*, 128, 279–301

Serafin, S., Adler, B., Cuxart, J., De Wekker, S., Gohm, A., Grisogono, B., Kalthoff, N., Kirshbaum, D., Rotach, M., Schmidli, J., Stiperski, I., Večenaj, Ž. and Zardi, D. (2018) Exchange processes in the atmospheric boundary layer over mountainous terrain. *Atmosphere*, 9, 1–32. https://doi.org/10.3390/atmos9030102

Silcox, G.D., Kelly, K.E., Crosman, E.T., Whiteman, C.D. and Allen, B.L. (2012) Wintertime PM$_2$.5 concentrations during persistent, multi-day cold-air pools in a mountain valley. *Atmospheric Environment*, 46, 17–24

Steyn, D.G., De Wekker, S.F., Kossmann, M. and Martilli, A. (2013). Boundary layers and air quality in mountainous terrain, in *Mountain Weather Research and Forecasting*, Chow, F., De Wekker, S.F., Snyder, B. (eds.), pp. 261–289. Springer, Dordrecht, Netherlands.

Tomasi, E., Giovannini, L., Zardi, D. and de Franceschi, M. (2017) Optimization of Noah and Noah_MP WRF land surface schemes in snow-melting conditions over complex terrain. *Monthly Weather Review*, 145, 4727–4745

VanReken, T.M., Dhammapala, R.S., Jobson, B.T., Bottenus, C.L., VanderSchelden, G.S., Kaspari, S.D., Gao, Z., Zhu, Q., Lamb, B.K., Liu, H. and Johnston, J. (2017) Role of persistent low-level clouds in mitigating air quality impacts of wintertime cold pool conditions. *Atmospheric Environment*, 154, 236–246. https://doi.org/10.1016/j.atmosenv.2017.01.043

Wagner, J., Gohm, A. and Rotach, M. (2015a) The impact of valley geometry on daytime thermally driven flows and vertical transport processes. *Quarterly Journal of the Royal Meteorological Society*, 141, 1780–1794

Wagner, J., Gohm, A. and Rotach, M. (2015b) Influence of along-valley terrain heterogeneity on exchange processes over idealized valleys. *Atmospheric Chemistry and Physics*, 15, 6589–6603

Whiteman, C.D. (2000) *Mountain Meteorology: Fundamentals and Applications*. Oxford University Press, Oxford, UK.

Whiteman, C.D., Hoch, S.W., Horel, J.D. and Charland, A. (2014) Relationship between particulate air pollution and meteorological variables in Utah's Salt Lake Valley. *Atmospheric Environment*, 94, 742–753

Whiteman, C.D., Zhong, S., Shaw, W.J., Hubbe, J.M., Bian, X. and Mittelstadt, J. (2001) Cold pools in the Columbia basin. *Weather and Forecasting*, 16, 432–447

Zardi, D. and Whiteman, C.D. (2013). Diurnal mountain wind systems in Mountain Weather Research and Forecasting, Chow, F., De Wekker, S.F., Snyder, B. (eds.), pp. 35–119. Springer, Dordrecht, Netherlands.